ACCEPTED FOR PUBLICATION IN THE ASTROPHYSICAL JOURNAL LETTERS
Preprint typeset using LaTeX style emulateapj v. 05/04/06

THE EXTENDED STAR FORMATION HISTORY OF THE ANDROMEDA SPHEROID AT TWENTY ONE KILOPARSECS ON THE MINOR AXIS[1,2]

THOMAS M. BROWN[3], ED SMITH[3], HENRY C. FERGUSON[3], PURAGRA GUHATHAKURTA[4], JASONJOT S. KALIRAI[4,5], R. MICHAEL RICH[6], ALVIO RENZINI[7], ALLEN V. SWEIGART[8], DAVID REITZEL[6], KAROLINE M. GILBERT[6], MARLA GEHA[9]

Accepted for publication in The Astrophysical Journal Letters

ABSTRACT

Using the *HST* ACS, we have obtained deep optical images of a southeast minor-axis field in the Andromeda Galaxy, 21 kpc from the nucleus. In both star counts and metallicity, this field represents a transition zone between the metal-rich, highly-disturbed inner spheroid that dominates within 15 kpc and the metal-poor, diffuse population that dominates beyond 30 kpc. The color-magnitude diagram reaches well below the oldest main-sequence turnoff in the population, allowing a reconstruction of the star formation history in this field. Compared to the spheroid population at 11 kpc, the population at 21 kpc is ∼1.3 Gyr older and ∼0.2 dex more metal-poor, on average. However, like the population at 11 kpc, the population at 21 kpc exhibits an extended star formation history; one third of the stars are younger than 10 Gyr, although only a few percent are younger than 8 Gyr. The relatively wide range of metallicity and age is inconsistent with a single, rapid star-formation episode, and instead suggests that the spheroid even at 21 kpc is dominated by the debris of earlier merging events likely occurring more than 8 Gyr ago.

Subject headings: galaxies: evolution – galaxies: stellar content – galaxies: halos – galaxies: individual (M31)

1. INTRODUCTION

According to hierarchical models of galaxy formation, spheroids form in a repetitive process during the merger of galaxies and protogalaxies, while disks form by the slow accretion of gas between these merging events (e.g., White & Frenk 1991). Hierarchical models based on cold dark matter have shown great success in reproducing the observable universe on scales larger than a Mpc, but these models can lead to a "missing satellite problem," with many more dwarf galaxies predicted than are actually seen around the Milky Way (Moore et al. 1999). In answer to this problem, Bullock, Kravtsov, & Weinberg (2000) suggested that after the reionization of the universe, photoionization suppressed gas accretion in subhalos, keeping most of them dark-matter dominated, while a large fraction of the subhalos that became dwarf galaxies were tidally disrupted into the halos of their parent galaxies. Grebel & Gallagher (2004) countered that the presence of ancient stars in all dwarf galaxies, along with their wide variety of star formation histories, is evidence against a dominant suppression from reionization. In any case, recent semi-analytical hierarchical models of spheroid formation have had some success in modeling the spheroids and satellites of large galaxies (e.g., Bullock & Johnston 2005).

The Andromeda Galaxy (NGC 224, M31) offers an ideal laboratory for testing these models. Because M31 is inclined nearly edge-on (12°; de Vaucouleurs 1958) at a distance of 770 kpc (Freedman & Madore 1990), wide surveys can map its morphology, metallicity, and kinematics (e.g., Ferguson et al. 2002; Kalirai et al. 2006), while deep color-magnitude diagrams (CMDs) can reveal its star-formation history (e.g., Brown et al. 2006; Olsen et al. 2006). Here we present a new deep CMD of a minor-axis field located 21 kpc from the M31 nucleus. Within 15 kpc is the metal-rich, highly-disturbed spheroid that has been the subject of numerous "halo" studies since the work of Mould & Kristian (1986). Beyond 30 kpc, two independent groups have recently discovered the spheroid more closely resembles a textbook spiral galaxy halo (Irwin et al. 2005; Guhathakurta et al. 2005), with lower metallicities and a r^{-2} power-law profile. Our new field falls in the transition zone between these two distinct regions: well beyond the tidal features present in the inner spheroid (Ferguson et al. 2002), but within that part of the spheroid exhibiting relatively high metallicities (Kalirai et al. 2006) and a de Vaucouleurs surface-brightness profile (Durrell et al. 2004).

2. OBSERVATIONS AND DATA REDUCTION

Using the Advanced Camera for Surveys (ACS) on the *Hubble Space Telescope (HST)*, we obtained deep optical images of a minor-axis field 1.5° (21 kpc) from the M31 nucleus, at $\alpha_{2000} = 00^h49^m05^s$, $\delta_{2000} = 40°17'37''$. The field falls outside of the disturbances seen in the Ferguson et al. (2002) star count map, including those revealed in the Sobel-filtered version by Fardal et al. (2006). The field lies a few arcmin beyond the "clean halo" fields of Ferguson et al. (2005), also observed with ACS but with less depth. The 21 kpc field is part of a new ACS program sampling the outer spheroid of M31; the remaining fields, falling ∼35 kpc from the nucleus, will be discussed in a later paper.

From 9–28 Aug 2006, we obtained 8 hours of images in the

[1] Based on observations made with the NASA/ESA Hubble Space Telescope, obtained at STScI, and associated with proposal 10816.

[2] Based on observations obtained at the W.M. Keck Observatory, which is operated by the California Institute of Technology, the University of California, and NASA, and made possible by the generous financial support of the W.M. Keck Foundation.

[3] Space Telescope Science Institute, 3700 San Martin Drive, Baltimore, MD 21218; tbrown@stsci.edu, edsmith@stsci.edu, ferguson@stsci.edu

[4] University of California Observatories / Lick Observatory, 1156 High Street, University of California, Santa Cruz, CA 95064; raja@ucolick.org, jkalirai@ucolick.org, kgilbert@ucolick.org

[5] Hubble Fellow

[6] Department of Physics and Astronomy, 430 Portola Plaza, Box 951547, University of California, Los Angeles, CA 90095; rmr@astro.ucla.edu, reitzel@ucla.astro.edu

[7] Osservatorio Astronomico, Vicolo Dell'Osservatorio 5, I-35122 Padova, Italy; arenzini@pd.astro.it

[8] Code 667, NASA Goddard Space Flight Center, Greenbelt, MD 20771; allen.v.sweigart@nasa.gov

[9] NRC Herzberg Institute of Astrophysics, 5071 West Saanich Road, Victoria BC V9E 2E7, Canada; Plaskett Fellow; marla.geha@nrc-cnrc.gc.ca

F606W filter (broad V) and 13 hours in the F814W filter (I) on the Wide Field Camera, with every exposure dithered to enable hot pixel removal, optimal point spread function (PSF) sampling, smoothing of spatial variation in detector response, and filling in the detector gap. Because our reduction process is the same used by Brown et al. (2006), we will only briefly summarize it here. The images were registered, rectified, rescaled to $0.03''$ pixel^{-1}, and coadded using the DRIZZLE package (Fruchter & Hook 2002), with rejection of cosmic rays and hot pixels. PSF-fitting photometry, using the DAOPHOT-II software of Stetson (1987), was corrected to agree with aperture photometry of isolated stars, with the zeropoints calibrated at the 1% level. The final catalog contains ≈12,500 stars (Figure 1). Our photometry is in the STMAG system: $m = -2.5\times \log_{10} f_\lambda - 21.1$. For those more familiar with the ABMAG system, ABMAG = STMAG -0.169 for m_{F606W}, and ABMAG = STMAG -0.840 mag for m_{F814W}. We performed extensive artificial star tests to characterize the photometric errors and completeness in the catalog. To avoid affecting the properties we were trying to measure, we added only 500 artificial stars per pass, but by using thousands of passes, the tests contain over 4 million artificial stars.

Spectroscopy of red giant branch (RGB) stars in our field provides kinematic context for the population. The velocities (Figure 1) were measured as part of an ongoing Keck/DEIMOS survey of RGB stars in the M31 spheroid (Gilbert et al., in prep.), sampling various radii to map the surface brightness profile, kinematic structure, and metallicity distribution. For details on target selection, data reduction, velocity fitting, and separation of foreground dwarfs from M31 giants, see Gilbert et al. (2006). Compared to the velocities in Brown et al. (2006), Figure 1*a* includes ∼50% more stars that were recovered by reprocessing the data from this field.

The CMD of our 21 kpc field is shallower and far less crowded than the CMDs of the inner spheroid, tidal stream, and outer disk obtained by Brown et al. (2006). Ideally, in our current program we would obtain the same depth and star counts, but the scarcity of stars in these fields forced us to investigate the trade-off between depth and star counts that could be achieved in a program of reasonable size. Through simulations, we found that we could determine the predominant star formation history even with one-tenth the number of stars and 0.2 mag less depth. The penalty is some loss of sensitivity to minority population components (e.g., few percent bursts), which we demonstrate below. Note that the loss of depth in our current observations is somewhat mitigated by the smaller crowding errors.

Another distinction between the fields in the current program and those in our earlier programs is the charge transfer inefficiency (CTI) of the ACS CCD, due to radiation damage. Brown et al. (2006) could find no evidence of CTI in the images of the inner spheroid, disk, and stream, presumably because the CTI was mitigated by the bright sky and crowded fields filling the CCD traps. In the current images of the outer spheroid, the CTI appears as obvious streaks trailing the stars. The appearance of CTI can be attributed to the fainter sky in August M31 observations (due to the larger Sun angle), the far lower crowding, and the CCD being 2 years older. We thus apply a CTI correction to our photometry, using the algorithm of Riess & Mack (2005). The correction makes stars at the turnoff ($m_{F814W} \approx 29$ mag) 0.04 mag brighter, on average; at $m_{F814W} \approx 28$ mag it is 0.02 mag, while at $m_{F814W} \approx 30$ mag it is nearly 0.08 mag. Note that the CTI correction is not applied to the artificial star tests, because artificial stars are not clocked across the detector. Because the correction makes the faint stars brighter, it has a small but noticeable effect on the star formation history fits (§3); if we neglected the correction, the 21 kpc population would appear to be 180 Myr older and 0.15 dex more metal-poor.

3. ANALYSIS

In Figure 1 we compare the spheroid populations at 21 kpc and 11 kpc. Both fields exhibit a broad velocity distribution around the M31 systemic velocity; neither field shows clear evidence of a dominant kinematically-cold component, as might be expected if there were a majority contribution from a single stream or from the disk. It is difficult to make a fair qualitative comparison of the populations in these fields if their CMDs are shown at their full depth. Thus, in Figure 1*e*, we show a simulation of how the 11 kpc population would appear if observed under the same conditions as the 21 kpc field (crowding errors, exposure time, and star counts). The simulation has two components: for faint stars ($m_{F814W} \geq 26.5$ mag for $-0.9 \leq m_{F606W} - m_{F814W} \leq -0.1$ mag, and all stars at $m_{F814W} \geq 28.0$ mag) the population is a realization of the best-fit model for the 11 kpc field (Brown et al. 2006), but scattered using the completeness and photometric errors derived for the 21 kpc field (based on the artificial star tests); for bright stars, the population is a random draw (without repeats) on PSF-fitting photometry for the 11 kpc field, using a subset of the images approximating the exposure time in the 21 kpc field. Two components properly account for the significant differences in crowding and completeness for the faint stars (the lower RGB, subgiant branch [SGB], and main sequence, which are well-matched by the models), and accurately reproduce the bright stars (the HB, asymptotic giant branch, and upper RGB, where the models are not as accurate).

From the comparison of the 11 kpc and 21 kpc fields, it is clear that the 21 kpc population is somewhat more metal-poor and older. The median RGB color is 0.02 mag bluer (at $m_{F814W} = 27$ mag) and the RGB bump (immediately below the HB) is 0.2 mag brighter, both of which indicate lower metallicities. Despite these lower metallicities, the SGB and main sequence turnoff are 0.1 mag fainter, indicating older ages. The HB stars fall mostly in the red clump, but the fraction of blue HB stars is twice as large, implying both older ages and lower metallicities. The red clump in the 21 kpc field does not have the obvious extension to brighter luminosities seen in the red clump of the 11 kpc field, implying the metal-rich stars in the 21 kpc field do not extend to the young ages seen in the 11 kpc field. The luminosity at the base of the red clump suggests that both fields are at approximately the same distance, and we will assume that in the fits below; if we assumed the distance to the 21 kpc population was larger due to flattening of the spheroid, our fits for the 21 kpc field would shift younger. The RGB in the 21 kpc population is intrinsically 7% broader (after accounting for measurement errors); this is primarily due to a larger fraction of metal-poor stars, but also due to the shifting of metal-rich stars to older ages. Still, the 11 kpc and 21 kpc populations are not completely distinct. Both fields exhibit a broad RGB, indicating a wide range of metallicities. When compared to the 47 Tuc ridge line (*curve*; Brown et al. 2005), both fields exhibit a brighter SGB and turnoff, implying intermediate-age stars are present.

To produce a quantitative fit to the star formation history in the 21 kpc field, we used the methodology of Brown et al. (2006) and the Starfish code of Harris & Zaritsky (2001). The isochrones come from VandenBerg, Bergbusch,

& Dowler (2006), but were transformed to the ACS bandpasses (Brown et al. 2005); the isochrones do not include core He diffusion, which, if present, would shift our ages ∼10% younger. We restricted the fits to the lower RGB, SGB, and upper main sequence, where the random and systematic errors are minimized. Specifically, the fit region was bounded by $26.5 \leq m_{F814W} \leq 30.0$ mag and $-0.9 \leq m_{F606W} - m_{F814W} \leq -0.1$ mag, but a small 0.1×0.2 mag section was masked where it overlaps with the blue HB. The region and mask were the same used in our earlier fits to the disk and stream (the fit region for the inner spheroid extended 0.5 mag fainter).

The quantitative fits agree well with the inspection of the CMDs. Figures 1*f* and 1*g* show the best-fit star formation histories for the populations at 11 kpc (Brown et al. 2006) and 21 kpc. Although the 21 kpc population spans a wide range of age and metallicity, it does not extend as young as the 11 kpc population, and there is more weight in the old metal-poor population. A third of the stars are younger than 10 Gyr; fits that omit such stars are excluded at the 8σ level, while fits that omit stars younger than 6 Gyr are excluded at the 3σ level. Fits that omit stars more metal-rich than [Fe/H]$= -0.5$ are excluded at the 3σ level, but the omission of supersolar stars reduces the fit quality by less than 1σ (the fitting algorithm can compensate with more weight at or just below solar metallicity). On average, the 21 kpc population is 0.2 dex more metal poor than the 11 kpc population (consistent with Kalirai et al. 2006) and 1.3 Gyr older. In Figure 1*h*, we show the fit to the CMD shown in Figure 1*e* (which simulates 11 kpc population as it would appear if observed in the conditions of the 21 kpc field). Although the CMD in Figure 1*e* is significantly degraded (compared to that in Figure 1*c*), it is clear that the predominant star formation history can still be recovered (i.e., the star formation history in Figure 1*h* looks very similar to that in Figure 1*f*).

4. SUMMARY AND DISCUSSION

The M31 spheroid exhibits an extended star formation history at 11 kpc and 21 kpc on the minor axis. Compared to the 11 kpc field, the 21 kpc field is 0.2 dex more metal-poor and 1.3 Gyr older, on average, but the most striking difference in these populations is the presence of stars younger than 8 Gyr. At 11 kpc, 26% of the stars are younger than 8 Gyr, but at 21 kpc, $\lesssim$5% of the stars are (Figure 1*f* and 1*g*).

Brown et al. (2006) found that the intermediate-age population at 11 kpc could not be explained by a large contribution from stars currently residing in the disk or a chance intersection with the orbit of the tidal stream. Our current study yields an additional constraint: the 11 kpc spheroid population does not look like a linear combination of the stream and 21 kpc spheroid populations. Although the best fit to the stream population implies it is ∼1 Gyr younger than the 11 kpc spheroid population (on average), only 20% of the stream population is younger than 8 Gyr; most of the stream stars are 8–10 Gyr old (see Brown et al. 2006, Figure 13). The similarities between the stream and 11 kpc field imply pollution of the inner spheroid by stream debris, consistent with current models and observations of the stream and associated features (e.g., Fardal et al. 2006; Gilbert et al., in prep.), but the larger fraction of stars younger than 8 Gyr in the 11 kpc field may indicate that the inner spheroid is also polluted with stars disrupted from the disk. It would be interesting to model the stream with a live disk that accounts for both dynamical friction in the stream and disruption of disk stars.

Although we cannot tie any particular sub-population to any particular cannibalized galaxy, the wide range of ages and metallicities in the spheroid offer strong support to the hierarchical model, with the spheroid comprised of dispersed satellite galaxies and possibly debris from impacts through the disk. However, our results are not necessarily consistent with all predictions from hierarchical semi-analytical models. Kalirai et al. (2006) have shown that there is a metallicity gradient in the spheroid, such that it becomes more metal-poor at increasing radii. With only two points, one cannot draw a definite trend, but our data are consistent with such a metallicity gradient, and also indicate that the spheroid becomes older at increasing radii. Hierarchical models predict that the spheroid forms inside-out (e.g., Bullock & Johnston 2005), so one might expect younger ages at larger radii. The caveat is that the age distribution in a disrupted satellite might not be strongly tied to the time of its disruption; the star formation history of the tidal stream shows no indication that its progenitor was disrupted within the last Gyr (Brown et al. 2006), despite n-body simulations which point to this timescale (e.g., Fardal et al. 2006; Font et al. 2006). It will be interesting to explore the age distribution beyond 30 kpc, to see if the trend for increasing age at increasing radii continues.

Support for proposal 10816 is provided by NASA through a grant from STScI, which is operated by AURA, Inc., under NASA contract NAS 5-26555. We acknowledge support from NSF grants AST-0307966/AST-0507483 (PG) and AST-0307931 (RMR), NASA/STScI grants GO-10265/GO-10816 (PG, RMR), and NASA Hubble Fellowship grant HF-01185.01-A (JSK). We are grateful to P. Stetson for his DAOPHOT code, to J. Harris for his Starfish code, and to K. Johnston, A. Font, and M. Fardal for interesting discussions.

REFERENCES

Brown, T.M., et al. 2005, AJ, 130, 1693
Brown, T.M., Smith, D., Ferguson, H.C., Rich, R.M., Guhathakurta, P., Renzini, A., Sweigart, A.V., & Kimble, R.A. 2006, ApJ, 652, 323
Bullock, J.S., & Johnston, K.V. 2005, ApJ, 635, 931
Bullock, J.S., Kravtsov, A.V., & Weinberg, D.H. 2000, ApJ, 539, 517
de Vaucouleurs, G. 1958, ApJ, 128, 465
Durrell, P.R., Harris, W.E., & Pritchet, C.J. 2004, AJ, 128, 260
Fardal, M.A., Guhathakurta, P., Babul, A., & McConnachie, A.W. 2006, MNRAS, submitted, astro-ph/0609050
Ferguson, A.M.N., Irwin, M.J., Ibata, R.A., Lewis, G.F., & Tanvir, N.R. 2002, AJ, 124, 1452
Ferguson, A.M.N., Johnson, R.A., Faria, D.C., Irwin, M.J., Ibata, R.A., Johnston, K.V., Lewis, G.F., & Tanvir, N.R. 2005, ApJ, 622, L109
Font, A.S., Johnston, K.V., Guhathakurta, P., Majewski, S.R., & Rich, R.M. 2006, AJ, 131, 1436
Freedman, W.L., & Madore, B.F. 1990, ApJ, 365, 186
Fruchter, A.S., & Hook, R.N. 2002, PASP, 114, 144
Gilbert, K.M., et al. 2006, ApJ, 652, 1188
Grebel, E.K., & Gallagher, J.S., III 2004, ApJ, 610, L89
Guhathakurta, P., et al. 2005, arXiv preprint (astro-ph/0502366)
Harris, J., & Zaritsky, D. 2001, ApJS, 136, 25
Irwin, M.J., Ferguson, A.M.N., Ibata, R.A., Lewis, G.F., & Tanvir, N.R. 2005, 628, L108
Kalirai, J.S., et al. 2006, ApJ, 648, 389
Moore, B., Ghigna, S., Governato, F., Lake, G., Quinn, T., Stadel, J., & Tozzi, P. 1999, ApJ, 524, L19
Mould, J., & Kristian, J. 1986, ApJ, 305, 591
Olsen, K.A.G., Blum, R.D., Stephens, A.W., Davidge, T.J., Massey, P., Strom, S.E., & Rigaut, F. 2006, AJ, 132, 271
Riess, A., & Mack, J. 2005, in Instrument Science Report ACS 2004-006
Stetson, P. 1987, PASP, 99, 191
White, S.D.M., & Frenk, C.S. 1991, ApJ, 379, 52
VandenBerg, D.A., Bergbusch, P.A., & Dowler, P.D. 2006, ApJS, 162, 375

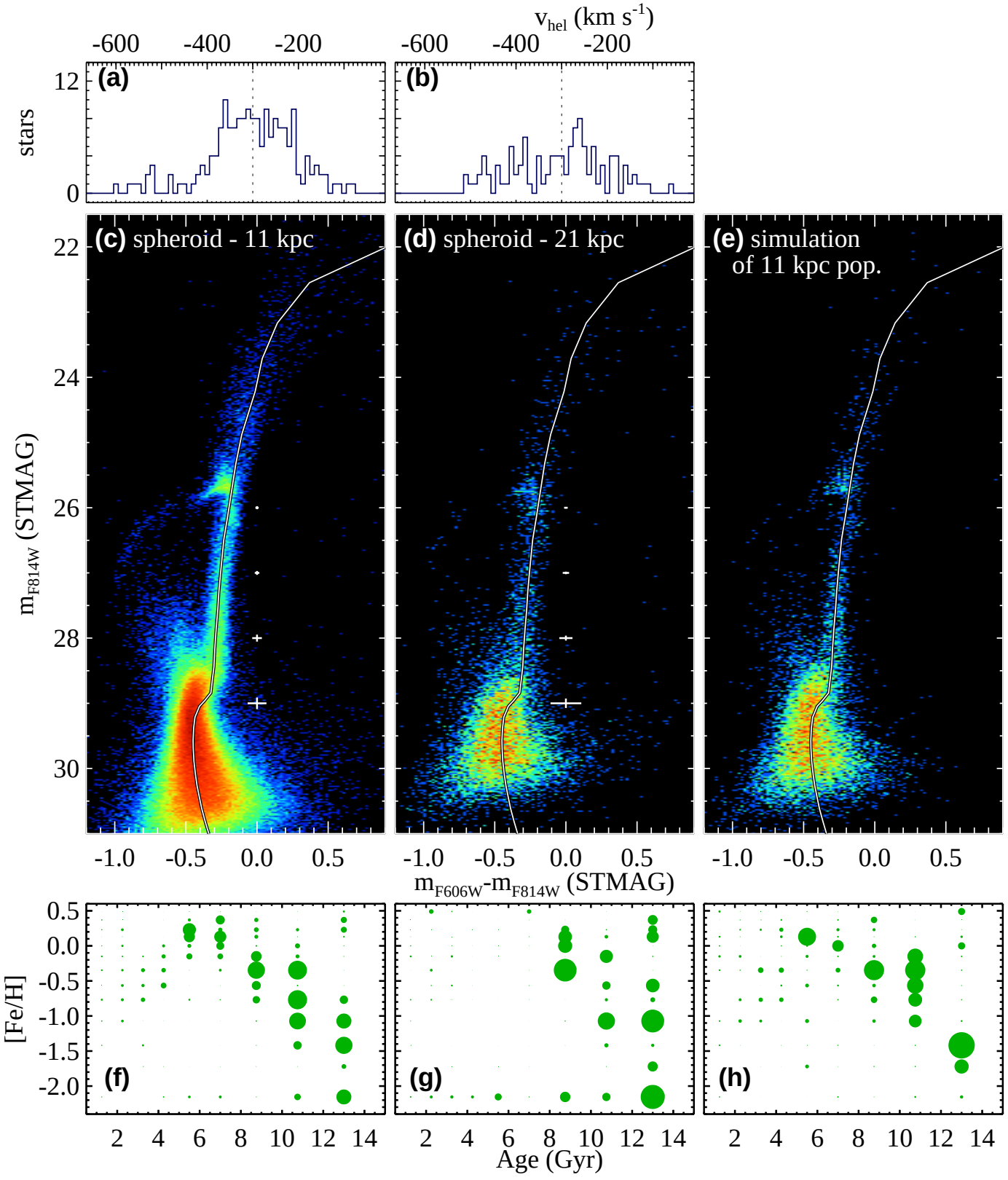

FIG. 1.— *(a)* Velocities for RGB stars within 9′ of our 11 kpc spheroid field, showing a broad distribution near the M31 systemic velocity (*dashed line*). *(b)* Velocities for RGB stars within 14′ of our 21 kpc spheroid field, also showing a broad distribution near the M31 systemic velocity. *(c)* The CMD of the spheroid population at 11 kpc. The ridge line of NGC 104 (*white curve*; Brown et al. 2005) is shown for comparison. *(d)* The same, but for the spheroid population at 21 kpc. *(e)* A simulation showing how the 21 kpc CMD (panel [*d*]) would appear if its population were identical to that at 11 kpc. *(f,g,h)* The best-fit star formation histories for the CMDs shown in panels *(c,d,e)*. The area of each filled circle is proportional to the number of stars at that age and metallicity. The 21 kpc field hosts a broad range of age and metallicity (panel [*g*]), but the population is older and more metal-poor than that in the 11 kpc field (panel [*f*]).